Phase competition and long-period charge/orbital ordering in the overdoped distorted perovskite manganites $R_{1-x}Sr_xMnO_3$

Y. Tomioka,[1] X. Z. Yu,[2] T. Ito,[1] Y. Matsui,[2] and Y. Tokura[3,4]

[1]*Nanoelectronic Research Institute (NeRI), National Institute for Advanced Industrial Science and Technology (AIST), 1-1-1 Higashi, Tsukuba 305-8562, Japan*

[2]*Advanced Nano Characterization Center (ANCC), National Institute for Materials Science (NIMS), Tsukuba 305-0044, Japan*

[3]*Department of Applied Physics, University of Tokyo, Hongo, Bunkyo-ku, Tokyo 113-8656, Japan*

[4]*Cross-Correlated Materials Research Group (CMRG), Advanced Science Institute (ASI), RIKEN, 2-1 Hirosawa, Wako, Saitama 351-0198, Japan*

(Received 29 April 2009; revised manuscript received 4 August 2009; published 14 September 2009)

For the manganites of $R_{1-x}Sr_xMnO_3$ (R=$Nd_{0.5}Sm_{0.5}$, Sm, and Eu), the new $q\sim1/3$ charge/orbital ordering with the orbital modulation vector of $(0, q, 0)$ in an orthorhombic *Pbnm* setting is observed at $0.5<x<0.6$, where the A-type antiferromagnetic state (x^2-y^2-type orbital order) is relatively reduced. The modulation is commensurate ($q=1/3$) upon the transition but turns into incommensurate ($q>1/3$) with lowering temperature. In these manganites, a competition is seen among the long (short)-ranged $q=1/3$ (1/2) charge/orbital ordering, the A-type and C-type antiferromagnetic phases.

DOI: 10.1103/PhysRevB.80.094406 PACS number(s): 75.30.Kz, 71.27.+a, 71.30.+h

I. INTRODUCTION

In the hole-doped manganese oxides with perovskite structure, $R_{1-x}AE_xMnO_3$ (R and AE being rare-earth and alkaline-earth elements, respectively), a competing feature is seen under a coupling among spin, charge, and orbital (lattice) degrees of freedom.[1–3] For $R_{1-x}Ca_xMnO_3$ with small quenched disorder,[4] in competition with metallic ferromagnetism due to the double exchange interaction,[5,6] charge/orbital ordering (CO/OO) (ordering of Mn^{3+}/Mn^{4+} with 1/1 accompanied by e_g-orbital ordering) occurs at $x\sim0.5$, in which the modulation vector, $(0, q, 0)$ in the orthorhombic *Pbnm* setting ($a_0\sim b_0\sim c_0/\sqrt{2}\sim\sqrt{2}a_p$, where a_p is the lattice parameter of the pseudocubic lattice) is expressed as $q=1/2$ for $x\leq0.5$ and $q=1-x$ for $x>0.5$.[7,8] For $La_{1-x}Ca_xMnO_3$ ($x\sim0.66$),[8–10] the $q=1/3$ CO/OO (an ordering of Mn^{3+}/Mn^{4+} with 1/2) has also been known and both "bistripe"[9] and "Wigner-crystal"[8,10] models have been proposed as a concrete pattern of the ordering. In the case of $La_{1-x}Ca_xMnO_3$ with the critical temperature for the $q=1/2$ CO/OO [$T_{CO}(q=1/2)$] as high as about 200 K, the A-type antiferromagnetic (AF) state does not appear for $x>0.5$ and the competition may occur between the $q=1/2$ CO/OO and the $q=1/3$ CO/OO, which makes the modulation incommensurate for $0.5<x<0.66$.

In $R_{1-x}Sr_xMnO_3$ (R=La, Pr, Nd, Sm, and Eu), on the other hand, a ferromagnetic metal (FM) successively changes to the layered (A-type) and chained (C-type) AF phase as x increases across 0.5, which is typically seen in the x-dependent electronic phase for $Nd_{1-x}Sr_xMnO_3$.[11,12] For $R_{1-x}Sr_xMnO_3$, therefore, the $q=1/3$ or $1-x(x>0.5)$ CO/OO has not been reported so far, although the $q=1/2$ CO/OO occurs for R=Nd and Sm at $x\sim0.5$.[13,14]

In this paper, we report an appearance of the CO/OO ($q\sim1/3$) at an overdoped regime ($0.5<x<0.6$) in $R_{1-x}Sr_xMnO_3$ (R=$Nd_{0.5}Sm_{0.5}$, Sm, and Eu), which is analogous to the $q=1/3$ CO/OO in $La_{1-x}Ca_xMnO_3$ ($x\sim0.66$).[8–10] In these manganites, the A-type AF state is suppressed so that the $q\sim1/3$ CO/OO assisted by an orthorhombic distortion becomes alternatively visible around $x=0.55$.

II. EXPERIMENTS

Single crystals of $R_{0.45}Sr_{0.55}MnO_3$ (R=$La_{0.5}Pr_{0.5}$, Pr, $Pr_{0.5}Nd_{0.5}$, Nd, $Nd_{0.5}Sm_{0.5}$, Sm, Eu, and Gd) have been prepared by the floating zone method, the detail of which was described in Ref. 14. The mixed powders of R_2O_3 (R=La, Nd, Sm, Eu, and Gd), Pr_6O_{11}, $SrCO_3$, and Mn_2O_3 with a prescribed ratio were first calcined at 1050–1100 °C for 12–24 h in air. The specimens were pulverized and again sintered in the same condition. Then, the powders were pressed into a rod with about 4 mm in diameter and about 50 mm in length. The rod was fired at 1300–1400 °C for 12–24 h in air. The crystal growth was performed in an oxygen atmosphere with rotating feed and seed rods in opposite directions. The growth rate was set at 5–20 mm/h. The obtained crystals were pulverized and checked by a powder x-ray diffraction (XRD) with Cu $K\alpha$ radiation (MXP18 AHF[22], MAC Science Co., Ltd.). The diffraction pattern was collected by the $\theta/2\theta$ step scanning method with ranging $15°\leq2\theta\leq110°$. Rietveld refinement of the XRD pattern indicated that the obtained crystal is of single phase. Magnetization was measured by a superconducting quantum interference device magnetometer and resistivity was measured in a cryostat equipped with a superconducting magnet. A single-crystal x-ray diffraction was performed using an imaging plate system with Mo $K\alpha$ radiation.[14] Electron-transparent thin samples were prepared by argon-ion thinning (an acceleration voltage of 4 kV at low temperature) followed by mechanical polishing. The selected-area electron-diffraction (SAED) pattern was obtained using a transmission electron microscopy (TEM) Hitachi HF-3000S with an acceleration voltage of 300 kV.

III. RESULTS AND DISCUSSION

The electronic phases of $Nd_{1-x}Sr_xMnO_3$ (left) (Refs. 11 and 12) and $Sm_{1-x}Sr_xMnO_3$ (right) are indicated in Fig. 1. In

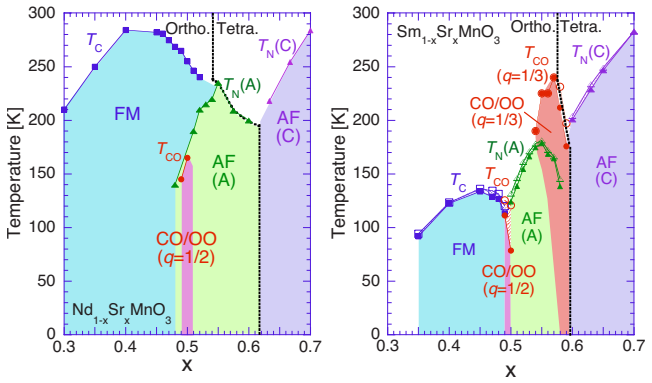

FIG. 1. (Color online) The x-dependent phase diagrams of $Nd_{1-x}Sr_xMnO_3$ (Refs. 11 and 12) (left) and $Sm_{1-x}Sr_xMnO_3$ (right). Ferromagnetic metal, charge/orbital ordering ($q=1/2$), A-type (layered) antiferromagnetic phase, charge/orbital ordering ($q=1/3$), and C-type antiferromagnetic phase are denoted as FM, CO/OO ($q=1/2$), AF(A), CO/OO ($q=1/3$) and AF(C), respectively. T_C, T_{CO}, T_N(A), $T_{CO}(q=1/3)$, and T_N(C) are the transition temperatures from (to) the respective phases, which are indicated by open (closed) squares, red circles, green triangles, red circles, and violet triangles, respectively. The boundaries between an orthorhombic and a tetragonal phases are denoted as dotted lines.

the manganites, the stability of FM or the A-type AF phase is scaled by the effective one-electron bandwidth of the e_g-band (W) (Ref. 15) that is controlled by the crystal lattice distortion[16] as quantified by the averaged radius (r_A) of the perovskite A-site cations; $r_A=(1-x)r_{RE3+}+xr_{Sr2+}$, where r_{RE3+} and r_{Sr2+} are the ionic radii of respective cations. In Fig. 1 (left), the critical temperatures for the FM (T_C) and the A-type AF phase [T_N(A)] are ~280 K at $0.4<x<0.45$ and 230 K at $x\sim0.55$, respectively, while in Fig. 1 (right) for further lattice-distorted manganites, $Sm_{1-x}Sr_xMnO_3$, those are lowered to ~130 K at $x\sim0.45$ and 180 K at $x\sim0.55$, respectively.[14]

In Fig. 1 (right), the crystal structure at room temperature is orthorhombic at $x\leq0.57$ while it is tetragonal at $x\geq0.58$. At the orthorhombic region of $0.54\leq x<0.6$ in Fig. 1 (right), the $q=1/3$ CO/OO appears above the A-type AF phase. At $x\geq0.6$, the $q=1/3$ CO/OO together with the lower A-type AF phase are abruptly replaced with the C-type AF phase in spite of that at $0.54\leq x\leq0.57$ the critical temperature for the $q=1/3$ CO/OO [$T_{CO}(q=1/3)$] increases with x. As a typical example, we show in Fig. 2 temperature profiles of (a) magnetization, (b) resistivity, (c) lattice parameters, and (d) an intensity of a superlattice (SL) for a $Sm_{1-x}Sr_xMnO_3$ ($x=0.57$) crystal. In Figs. 2(a)–2(c), a decrease in magnetization around 200 K, a peak in resistivity at 180 K, and elongations of a and b axes together with the contraction of c axis around 200 K are seen, respectively, which are all indicative of the onset of the A-type AF phase. In Fig. 2(d), however, a SL spot becomes visible around 225 K [inset (right)], the position of which is between (0 2 0) and (1/2 3/2 0), i.e., (ε/2 2-ε/2 0) with $\varepsilon\sim1/3$ of the pseudocubic setting and hence corresponds to the $q\sim1/3$ diffraction. As shown in Fig. 2(d), the intensity of SL first increases as temperature decreases. Below about 180 K, however, the A-type AF phase starts to appear and weaken the $q=1/3$ CO/OO. As

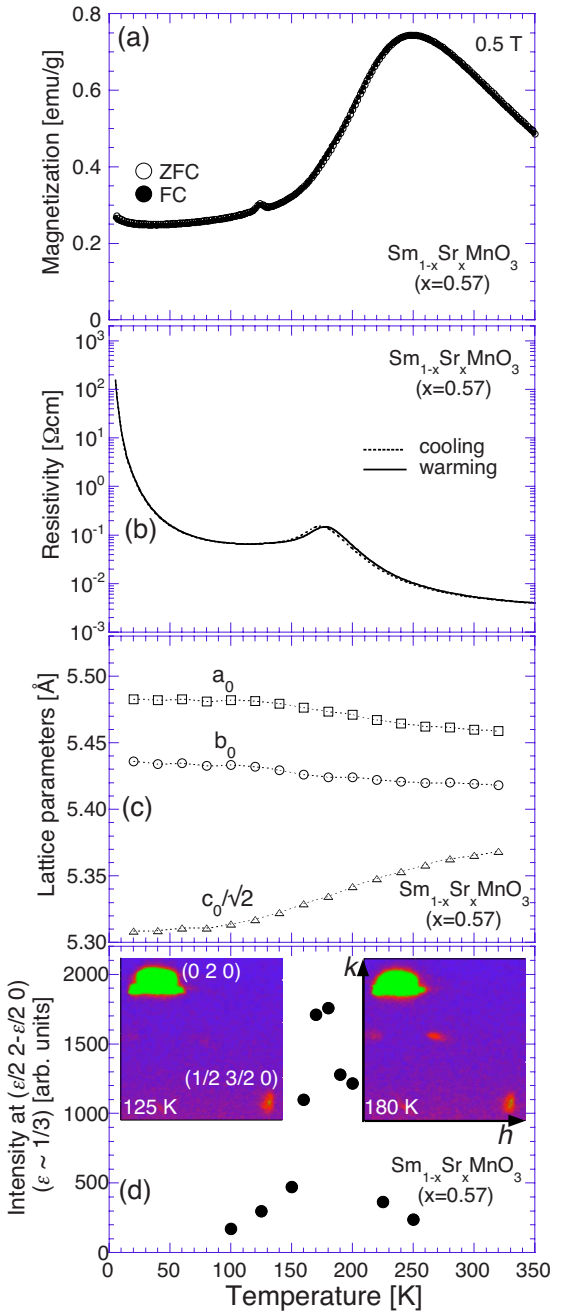

FIG. 2. (Color online) Temperature profiles of (a) magnetization, (b) resistivity, (c) lattice parameters, and (d) the peak intensity of a superlattice at (ε/2 2-ε/2 0) with $\varepsilon\sim1/3$ of the pseudocubic setting for the $x=0.57$ crystal, respectively. In (c), the orthorhombic axes are indexed as $Pbnm$ ($a_0\sim b_0\sim c_0/\sqrt{2}\sim\sqrt{2}a_p$, where a_p is the lattice parameter of the pseudocubic lattice). Insets (left, right) are the single-crystal x-ray diffraction patterns at (125 K, 180 K).

temperature further decreases below 100 K, the SL intensity becomes almost zero [inset (left)]. For $x=0.57$, therefore, the $q=1/3$ CO/OO appears above T_N(A) and is subsequently replaced with the A-type AF phase as temperature decreases.

Figure 3 shows the versions for the crystals of [(a)–(d)] $x=0.54$ and [(e)–(h)] 0.59, respectively. In Fig. 3(d), intensity of x-ray diffuse scattering at (0.15 1.85 0) is also indicated, which is estimated by fitting the profile of (0.15

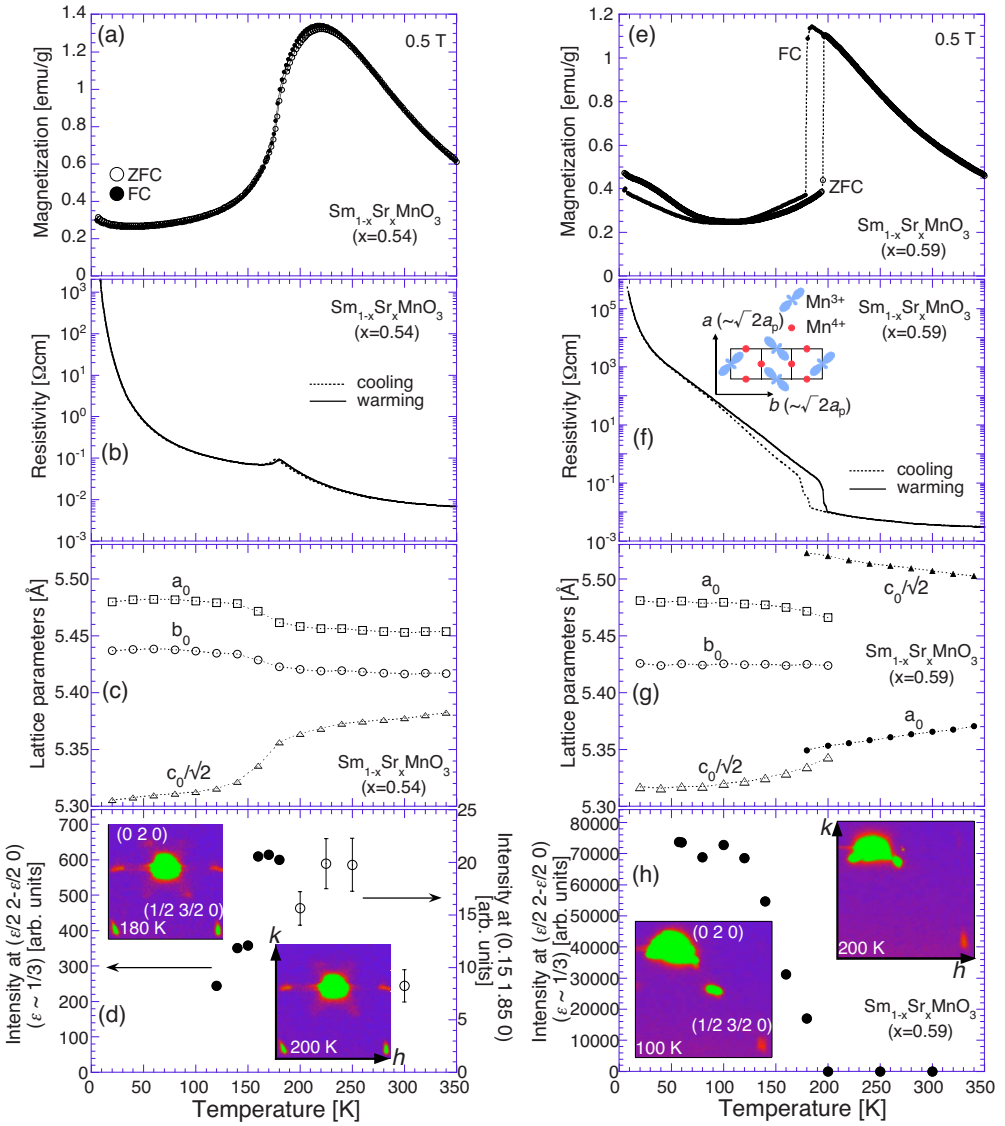

FIG. 3. (Color online) Temperature profiles of [(a) and (e)] magnetization, [(b) and (f)] resistivity, [(c) and (g)] lattice parameters, and [(d) and (h)] the intensity of x-ray diffuse scattering at (0.15 1.85 0) as well as the peak intensity of a superlattice at ($\varepsilon/2$ 2-$\varepsilon/2$ 0) with $\varepsilon \sim 1/3$ of the pseudocubic setting for the [(a)–(d)] $x=0.54$ and [(e)–(h)] 0.59 crystals, respectively. In (c) and (g), the orthorhombic (tetragonal) axes are indexed as *Pbnm* ($a_0 \sim b_0 \sim c_0/\sqrt{2} \sim \sqrt{2}a_p$, where a_p is the lattice parameter of the pseudocubic lattice) [*I*4/*mcm* ($a_0 \sim \sqrt{2}a_p$ and $c_0 \sim 2a_p$)]. Insets (left, right) are the single-crystal x-ray diffraction patterns at (180 K, 200 K) and (100 K, 200 K) for (d) $x=0.54$ and (h) 0.59, respectively. Reflections at both left and right sides of (0 2 0) in the insets of (d) are due to a twinning of the crystal. A structure of charge/orbital ordering ($q=1/3$) [Wigner-crystal model (Refs. 8 and 10)] in the orthorhombic *Pbnm* setting is schematically drawn in the inset of (f).

$+\delta/2$ $1.85+\delta/2$ 0) ($-0.5 \leq \delta \leq 0.5$) with a Gaussian form.[14] In Figs. 3(a)–3(c), similarly to Figs. 2(a)–2(c), a decrease in magnetization, a peak in resistivity, and elongations of *a* and *b* axes together with the contraction of *c* axis at ~180 K are seen, respectively, which are indicative of the A-type AF phase accompanied by the ferroic x^2-y^2-type orbital order. In Fig. 3(d), a diffuse scattering at (0.15 1.85 0), i.e., the $q=1/2$ CO/OO in a short range,[17] is visible above T_N(A), as shown in the inset (right). As temperature decreases in Fig. 3(d), however, the edge of the diffuse scattering is intensified and changes to a SL spot, as shown in the inset (left). As temperature further decreases below T_N(A), however, the intensity decreases and it is almost zero below 100 K. For $x=0.54$, therefore, the $q=1/2$ CO/OO in a short range and the $q=1/3$ CO/OO appear successively, which is replaced with the A-type AF phase as temperature further decreases.

For $x=0.59$, as indicated in Figs. 3(e) and 3(f), a drop (jump) in the field-cooled (FC) [zero-field-cooled (ZFC)] magnetization and an increase (decrease) in resistivity in a cooling (warming) run at around 190 K are seen, respectively. These changes are ascribed to a structural change between tetragonal[18,19] and orthorhombic at around 190 K, as indicated in Fig. 3(g). In Fig. 3(h), there is no observed SL spot in the tetragonal phase while there is in the orthorhombic one, as shown in the insets (left and right). It is also noted that intensity of the SL remains finite down to the lowest

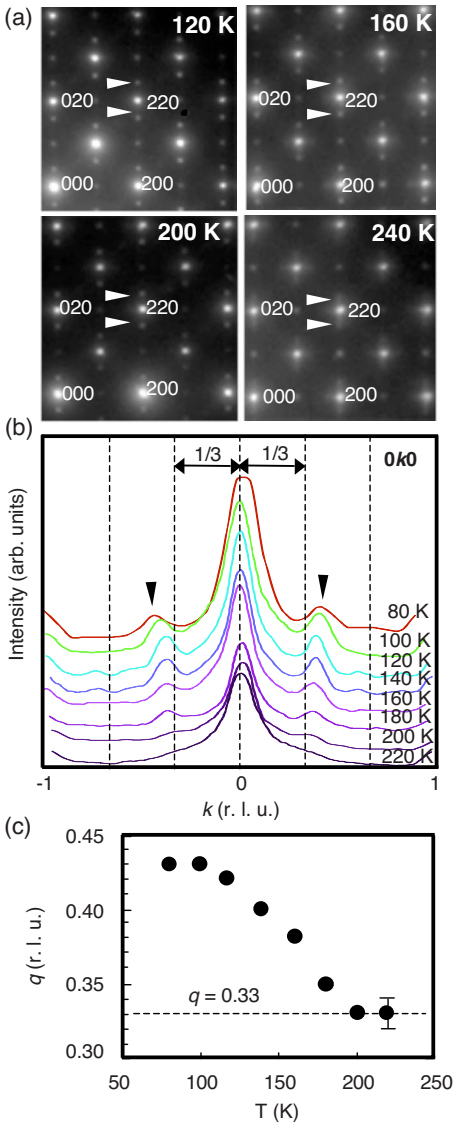

FIG. 4. (Color online) (a) SAED patterns at 240, 200, 160, and 120 K, (b) intensity profiles of 0*k*0 scan (in the orthorhombic *Pbnm* setting) with varying temperatures, and (c) temperature evolutions of the modulation vector for a $Sm_{1-x}Sr_xMnO_3$ (x=0.56) crystal, respectively (Ref. 20).

temperature (57 K), being different from the cases of x =0.54 [Fig. 3(d)] and 0.57 [Fig. 2(d)].

Figure 4 shows (a) the SAED patterns (at 240, 200, 160, and 120 K), (b) temperature evolutions of intensity profiles of the 0*k*0 scan (orthorhombic *Pbnm* setting), and (c) those of the modulation vector for a $Sm_{1-x}Sr_xMnO_3$ (x=0.56) crystal, respectively.[20] In Fig. 4(a), SL spots at $(0 \pm \varepsilon 0)$ ($\varepsilon \sim 1/3$) are distinctly seen below 200 K, where ε is temperature dependent as seen in Figs. 4(b) and 4(c); ε is nearly 1/3 at 200 K but it gradually increases as temperature decreases. Namely, the modulation of CO/OO is commensurate (q=1/3) upon the transition but turns incommensurate ($q \sim 1-x$) at lower temperatures. Such a crossover from commensurate to incommensurate as shown in Figs. 4(b) and 4(c) is analogous to the case of the charge ordering (charge stripe) in the layered nickelates, $La_{2-x}Sr_xNiO_4$ with x around 1/3.[21]

A phase separation, i.e., a mixing in nanoscale of the q=1/2 CO/OO and the q=1/3 CO/OO below $T_{CO}(q=1/3)$ might also cause a crossover from commensurate to incommensurate.[20] Since the real space TEM image is for a quite narrow area of a small piece of the crystal, and both electron and x-ray diffraction patterns do not indicate that two superlattices appear at commensurate positions of $(\pm\varepsilon/2\ \ 2\text{-}\varepsilon/2\ \ 0)$ with ε=1/2 and 1/3, however, the phase separated state or the mixing might not be so stable as the bulk property. Further investigations seem to be needed to exactly identify the origin of the crossover behavior.

Figure 5 shows temperature profiles of resistivity for the crystals of $R_{0.45}Sr_{0.55}MnO_3$ (R=$Nd_{0.5}Sm_{0.5}$, Sm, Eu, and Gd) (a), temperature evolutions of intensity of x-ray diffuse scattering at (–0.15 1.85 0) for R=Gd (b) and Eu (c), and those of SL spots at $(\pm\varepsilon/2\ \ 2\text{-}\varepsilon/2\ \ 0)$ with $\varepsilon \sim 1/3$ for R=Eu (c), Sm (d), and $Nd_{0.5}Sm_{0.5}$ (e), respectively. Appearance of the A-type AF phase is manifested by a peak of resistivity [Fig. 5(a)], the temperature of which decreases from ~210 to ~130 K as R changes from $Nd_{0.5}Sm_{0.5}$ to Gd. For the crystals of R=$Nd_{0.5}Sm_{0.5}$ (e) and Sm (d), the SL starts to be seen just above T_N(A) as shown in the insets (right) of Figs. 5(d) and 5(e). As temperature decreases below T_N(A), however, the intensity is decreased by appearance of the A-type AF phase and it becomes almost zero at lower temperatures as shown in the insets (left). For R=Gd (b), only the diffuse scattering is seen below 250 K [inset (right)], the intensity of which is weakened by appearance of the A-type AF phase at ~130 K [inset (left)]. It is noted in Fig. 5(b) that the q=1/3 CO/OO does not appear, which might be ascribed to an effect of larger quenched disorder[4] on the competition between the A-type AF phase and the q=1/3 CO/OO, being analogous to that on the competition between the FM and the q=1/2 CO/OO.[22] For R=Eu (c), similarly to the case of R=Gd, the diffuse scattering is seen at 200 K$<T<$250 K [inset (right)] while it changes to the SL spot below 190 K [inset (left)]. Similarly to Figs. 5(d) and 5(e), the intensity begins to steeply decrease below 160 K, at which the A-type AF phase appears.

The inset of Fig. 5(a) indicates a phase diagram as a function of r_A for the crystals of $R_{1-x}Sr_xMnO_3$ (x=0.55) with R varying from $La_{0.5}Pr_{0.5}$ to Gd. The q=1/3 CO/OO appears for the moderately distorted orthorhombic crystals of R =$Nd_{0.5}Sm_{0.5}$, Sm, and Eu while it does neither for R=Gd nor the tetragonal crystals of R=$La_{0.5}Pr_{0.5}$, Pr, and Nd (although the crystal of R=Nd undergoes a transition from tetragonal to orthorhombic upon the appearance of the A-type AF phase[23]). As r_A further increases in the tetragonal crystals, such as R=$La_{0.5}Pr_{0.5}$, the A-type AF phase starts to be taken over by the FM.

IV. SUMMARY

In summary, it has been found that the charge and orbital ordering ($q \sim 1/3$) with the respective modulation vectors of $(q,q,0)$ and $(q/2,q/2,0)$ in the pseudocubic setting appears at an overdoped regime ($0.5<x<0.6$) in distorted perovskite manganites, $R_{1-x}Sr_xMnO_3$ (R=$Nd_{0.5}Sm_{0.5}$, Sm, and Eu). In these crystals, the critical temperature for the A-type

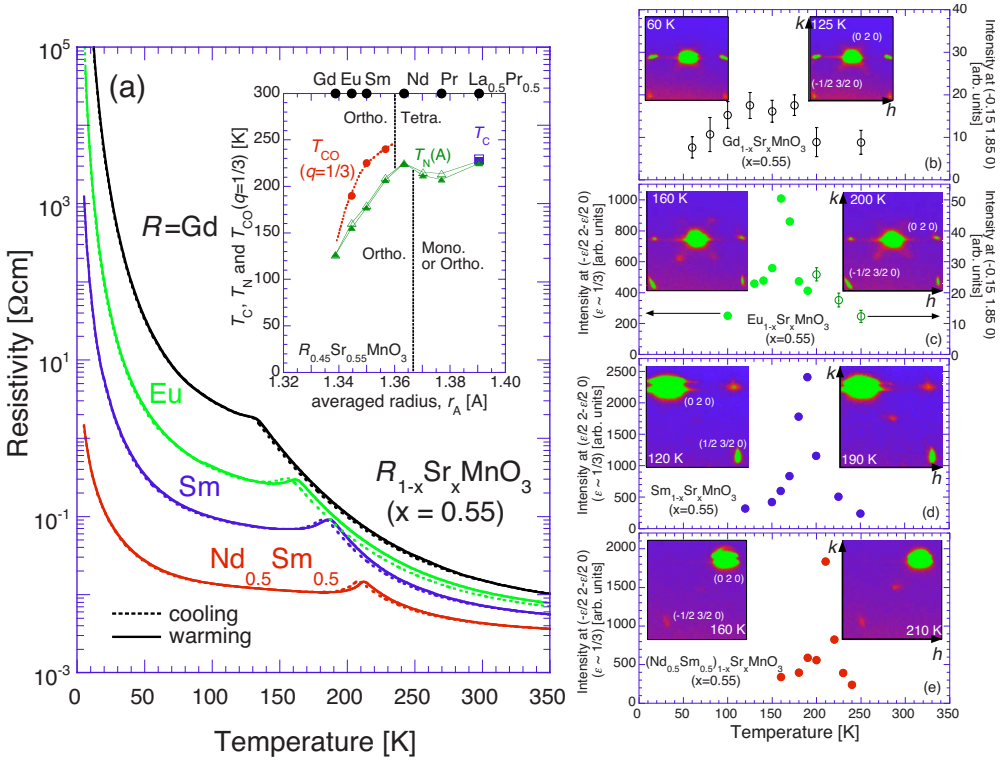

FIG. 5. (Color online) Temperature profiles of resistivity for the crystals of $R_{0.45}Sr_{0.55}MnO_3$ (R=$Nd_{0.5}Sm_{0.5}$, Sm, Eu, and Gd) (a), temperature evolutions of an intensity of an x-ray diffuse scattering at (−0.15 1.85 0) for R=Gd (b) and Eu (c), and those of an intensity of a superlattice at ($\pm\varepsilon/2$ 2-$\varepsilon/2$ 0) with $\varepsilon\sim1/3$ of the pseudocubic setting for R=Eu (c), Sm (d), and $Nd_{0.5}Sm_{0.5}$ (e), respectively. Inset of (a) shows T_C, T_N(A), and $T_{CO}(q=1/3)$ as a function of r_A for the crystals of $R_{0.45}Sr_{0.55}MnO_3$ (R=$La_{0.5}Pr_{0.5}$, Pr, $Pr_{0.5}Nd_{0.5}$, Nd, $Nd_{0.5}Sm_{0.5}$, Sm, Eu, and Gd). For R=$La_{0.5}Pr_{0.5}$, Pr, and $Pr_{0.5}Nd_{0.5}$, the crystal structure for $T<T_N$(A) is monoclinic $P2_1/n$ (Refs. 24 and 25) or orthorhombic *Fmmm* (Refs. 18 and 19). Insets (left, right) are single-crystal x-ray diffraction patterns at (60 K, 125 K), (160 K, 200 K), (120 K, 190 K), and (160 K, 210 K) for R=Gd (b), Eu (c), Sm (d), and $Nd_{0.5}Sm_{0.5}$ (e), respectively. Reflections at both left and right sides of (0 2 0) in the insets of (b)–(d) are due to a twinning of the crystal.

antiferromagnetic phase is lowered due to the narrowed bandwidth of the e_g band while the charge/orbital ordering ($q=1/3$) becomes alternatively visible at temperatures above the A-type antiferromagnetic phase as assisted by orthorhombic lattice distortion. The modulation of charge/orbital ordering is commensurate ($q=1/3$) upon the transition while it turns into incommensurate with decrease in temperature. It has been clarified that the distorted perovskite manganites with $x>0.5$ are under multicritical competition among the charge/orbital ordering ($q=1/2$) in a short range, the charge/orbital ordering ($q=1/3$), the A-type and the C-type antiferromagnetic states.

[1] Y. Tokura and N. Nagaosa, Science **288**, 462 (2000).
[2] E. Dagotto, T. Hotta, and A. Moreo, Phys. Rep. **344**, 1 (2001).
[3] Y. Tokura, Rep. Prog. Phys. **69**, 797 (2006).
[4] L. M. Rodriguez-Martinez and J. P. Attfield, Phys. Rev. B **54**, R15622 (1996).
[5] P. W. Anderson and H. Hasegawa, Phys. Rev. **100**, 675 (1955).
[6] P.-G. de Gennes, Phys. Rev. **118**, 141 (1960).
[7] G. C. Milward, M. J. Calderon, and P. B. Littlewood, Nature (London) **433**, 607 (2005).
[8] C. H. Chen, S.-W. Cheong, and H. Y. Hwang, J. Appl. Phys. **81**, 4326 (1997).
[9] S. Mori, C. H. Chen, and S.-W. Cheong, Nature (London) **392**, 473 (1998).
[10] P. G. Radaelli, D. E. Cox, L. Capogna, S.-W. Cheong, and M. Marezio, Phys. Rev. B **59**, 14440 (1999).
[11] R. Kajimoto, H. Yoshizawa, H. Kawano, H. Kuwahara, Y. Tokura, K. Ohoyama, and M. Ohashi, Phys. Rev. B **60**, 9506 (1999).
[12] H. Kuwahara, T. Okuda, Y. Tomioka, T. Kimura, A. Asamitsu, and Y. Tokura, in *Science and Technology of Magnetic Oxides*, edited by M. Hundley, J. Nickel, R. Ramesh, and Y. Tokura, MRS Symposia Proceedings Vol. 494 (Materials Research Society, Warrendale, PA, 2007), p. 83.
[13] H. Kuwahara, Y. Tomioka, A. Asamitsu, Y. Moritomo, and Y. Tokura, Science **270**, 961 (1995).
[14] Y. Tomioka, H. Hiraka, Y. Endoh, and Y. Tokura, Phys. Rev. B **74**, 104420 (2006).
[15] N. Furukawa, J. Phys. Soc. Jpn. **64**, 2754 (1995).
[16] J. B. Torrance, P. Lacorre, A. I. Nazzal, E. J. Ansaldo, and Ch. Niedermayer, Phys. Rev. B **45**, 8209 (1992).

[17] S. Shimomura, N. Wakabayashi, H. Kuwahara, and Y. Tokura, Phys. Rev. Lett. **83**, 4389 (1999).
[18] A. Sundaresan, V. Caignaert, B. Raveau, and E. Suard, Solid State Commun. **104**, 489 (1997).
[19] F. Damay, C. Martin, M. Hervieu, A. Maignan, B. Raveau, G. Andre, and F. Boure, J. Magn. Magn. Mater. **184**, 71 (1998).
[20] X. Z. Yu, Y. Tomioka, T. Asaka, K. Kimoto, T. Arima, Y. Tokura, and Y. Matsui, Appl. Phys. Lett. **94**, 082509 (2009).
[21] K. Ishizaka, T. Arima, Y. Murakami, R. Kajimoto, H. Yoshizawa, N. Nagaosa, and Y. Tokura, Phys. Rev. Lett. **92**, 196404 (2004).
[22] Y. Tomioka and Y. Tokura, Phys. Rev. B **70**, 014432 (2004).
[23] H. Kuwahara, T. Okuda, Y. Tomioka, A. Asamitsu, and Y. Tokura, Phys. Rev. Lett. **82**, 4316 (1999).
[24] H. Kawano, R. Kajimoto, H. Yoshizawa, Y. Tomioka, H. Kuwahara, and Y. Tokura, Phys. Rev. Lett. **78**, 4253 (1997).
[25] A. Llobet, J. L. Garcia-Munoz, C. Frontera, and C. Ritter, Phys. Rev. B **60**, R9889 (1999).